Fluid Dynamics & Materials Processing

Tech Science Press

DOI: 10.32604/fdmp.2024.054469

ARTICLE

A New Approach for the Calculation of Slope Failure Probability with Fuzzy Limit-State Functions

Jianing Hao[1], Dan Yang[2], Guanxiong Ren[1], Ying Zhao[3] and Rangling Cao[4,*]

[1]Department of Engineering Management, Sichuan College of Architectural Technology, Deyang, 61800, China

[2]Department of Transport and Municipal Engineering, Sichuan College of Architectural Technology, Deyang, 61800, China

[3]Department of Basic Teaching, Sichuan College of Architectural Technology, Deyang, 61800, China

[4]Sichuan Hongye Construction Software Co., Ltd., Chengdu, 610081, China

[*]Corresponding Author: Rangling Cao. Email: hy_crl2405@outlook.com

Received: 29 May 2024 Accepted: 06 November 2024 Published: 24 January 2025

ABSTRACT

This study presents an innovative approach to calculating the failure probability of slopes by incorporating fuzzy limit-state functions, a method that significantly enhances the accuracy and efficiency of slope stability analysis. Unlike traditional probabilistic techniques, this approach utilizes a least squares support vector machine (LSSVM) optimized with a grey wolf optimizer (GWO) and K-fold cross-validation (CV) to approximate the limit-state function, thus reducing computational complexity. The novelty of this work lies in its application to one-dimensional (1D), two-dimensional (2D), and three-dimensional (3D) slope models, demonstrating its versatility and high precision. The proposed method consistently achieves error margins within 3% of Monte Carlo simulation (MCS) results, while substantially reducing computation time, particularly for 2D and 3D models. This makes the approach highly practical for real-world engineering applications. Furthermore, by applying fuzzy mathematics to handle uncertainties in geotechnical properties, the method offers a more realistic and comprehensive understanding of slope stability. As water is the main factor influencing the stability of slopes, this aspect is investigated by calculating the phreatic line after the change in water level. Relevant examples are used to show that the failure probability of a slope under water wading condition can increase by more than 20% (increase rates in 1D, 2D and 3D conditions being 25%, 27% and 31%, respectively) compared with the natural condition. The influence of diverse fuzzy membership functions—linear, normal, and Cauchy—on failure probability is also considered. This research not only provides a strategy for better calculation of the slope failure probability but also pioneers the integration of computational intelligence, fuzzy logic and fluid-dynamics in geotechnical engineering, presenting an innovative and efficient tool for slope stability analysis.

KEYWORDS

Least Squares Support Vector Machine (LSSVM); Grey Wolf Optimizer (GWO); slope stability analysis; fuzzy set theory; failure probability estimation

1 Introduction

Failure probability is a critical metric in the assessment of slope stability, providing essential insights into the potential risk of slope failure [1]. This probability is derived from the inherent uncertainties present in geotechnical mechanical properties, which are primarily influenced by measurement errors and statistical variability.

Currently, probabilistic methods are the primary approach for calculating slope failure probability, largely due to the thorough theoretical development of probabilistic frameworks. These methods are broadly categorized into sampling methods and approximation methods, each with distinct advantages and limitations. MCS is the predominant sampling method employed in this domain. MCS is highly regarded for its accuracy, as it provides a precise probability calculation by simulating numerous possible scenarios. However, a significant drawback of MCS is its computational intensity, especially when dealing with complex limit-state functions [2]. In contrast, approximation methods, such as the first-order first-moment method [3] and the second-order second-moment method [4], offer faster calculations. These methods leverage Taylor series expansions to approximate the failure probability, which significantly reduces computation time. The trade-off, however, is that these methods can incur larger errors when applied to more complex limit-state functions. This discrepancy arises because the approximation may not capture the intricacies of the actual failure mechanisms accurately. To address the computational challenges associated with traditional methods, researchers have explored the integration of computational intelligence technologies. These advanced methods aim to replace or augment complex limit-state functions, thereby reducing computational costs while maintaining accuracy. Notable among these are neural networks [5], which have demonstrated substantial potential in pattern recognition and predictive modeling. Additionally, Kriging techniques [6,7], originally developed for geostatistical applications, have been adapted to estimate failure probabilities by interpolating the outputs of complex models. By leveraging the strengths of these computational intelligence methods, it is possible to achieve a balance between accuracy and computational efficiency. This hybrid approach allows for the effective handling of complex geotechnical data, thereby enhancing the reliability of slope stability analyses.

Fuzzy theory has also been utilized in the computation of failure probabilities for slopes and landslides. These approaches employ fuzzy sets to depict uncertain parameters, facilitating a more supple manifestation of the inherent variability in geotechnical properties [8–12]. Through the employment of fuzzy operations, failure probabilities of slopes can be estimated from a distinct perspective in contrast to traditional probabilistic methods. The considerable advantage of fuzzy sets over probabilistic theory resides in their capacity to capture the distribution of uncertain parameters more effectively, offering a more detailed comprehension of the variability and risks involved [13–15]. Nevertheless, there are prominent challenges related to the application of fuzzy sets in this context. A significant issue is the computational intricacy introduced by fuzzy arithmetic operations. A critical study conducted by Sotoudeh-Anvari [16] highlights that "current fuzzy mathematics is not even in a position to tackle reliably the simplest equations and consequently." This statement underscores the difficulties faced when performing basic arithmetic operations with fuzzy sets. While addition and subtraction are generally handled with sufficient accuracy, multiplication and division remain controversial and prone to significant errors. These technical challenges necessitate a cautious approach when employing fuzzy sets for slope failure probability estimation. It is essential to recognize the limitations and potential inaccuracies that can arise from the use of fuzzy arithmetic.

In addition to the inherent uncertainty of geological properties, the limit state function itself exhibits a degree of "uncertainty." Traditionally, many methods have strictly separated the safety and unsafety regions with a critical value of 1, designating areas with a safety factor greater than 1 as safe and those with a factor of 1 or less as unsafe. However, this binary classification does not align with engineering practice, where the reality is often more nuanced. In practice, a slope may remain stable even when the safety factor is slightly above 1, and conversely, it may fail when the safety factor is equal to or less than 1 [17]. This discrepancy highlights the existence of an intermediate state between the safety and unsafety regions, known as the "fuzzy area." The fuzzy area represents a zone where the slope has a certain possibility of instability, acknowledging the gradation of risk rather than a strict threshold (Fig. 1). Incorporating this ambiguity into the limit state function provides a more realistic and practical assessment of slope stability, reflecting the true nature of geotechnical uncertainties. Considering the ambiguity of the limit state function not only aligns the analysis closer to real-world conditions but also helps avoid the confusing calculations often associated with the concentration of ambiguity in fuzzy sets. This approach allows for a more nuanced and accurate representation of slope stability, recognizing that safety and failure are not always absolute states but exist on a spectrum influenced by various factors. To address these complexities, advanced methods that incorporate fuzzy logic and other computational techniques are necessary. These methods can effectively capture the intermediate state and provide a more comprehensive understanding of the slope's stability profile. By acknowledging and integrating the fuzzy area, engineers and researchers can develop more robust models that better predict the behavior of slopes under various conditions, ultimately leading to safer and more reliable geotechnical designs.

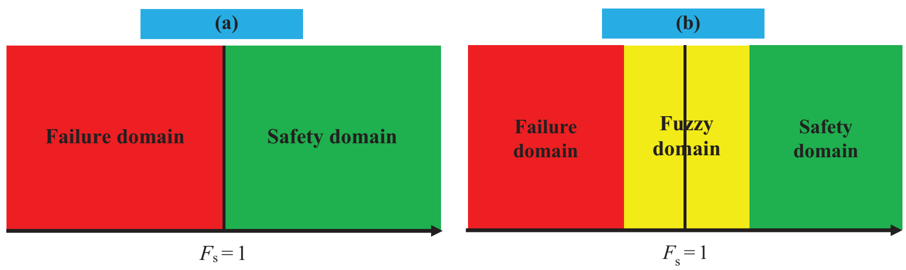

Figure 1: Definition of safety domain and failure domain: (a) without considering the fuzzification of limit-state function, and (b) considering limit-state function's fuzzification

The primary contribution of this article is the development of a novel method for calculating failure probability that incorporates the ambiguity of the limit-state function. Traditional methods often struggle with the binary classification of slope stability, which fails to capture the nuanced nature of geotechnical uncertainties. To address this, we propose a method that leverages a LSSVM [18], optimized by the GWO [19] and validated using the K-fold cross-validation technique [20]. This approach aims to provide a more flexible and accurate estimation of failure probabilities by integrating the inherent ambiguities within the limit-state function. The proposed algorithm stands out due to its universal applicability across various slope stability scenarios. By combining LSSVM with GWO, we enhance the optimization process, ensuring that the model parameters are fine-tuned for the best possible performance. The use of K-fold cross-validation further strengthens the model's reliability by systematically evaluating its predictive capability across multiple subsets of the data. To demonstrate the efficacy and robustness of our method, we conducted comprehensive analyses on one-dimensional (1D), two-dimensional (2D), and three-dimensional (3D) slope models [21].

The rest of this paper is organized as follows. In Section 2, a new calculation method of failure probability is derived and the detailed calculation flow is given. In Section 3, the proposed method is applied to three practical examples, and compared with MCS, which is the most accurate method for calculating the failure probability, the influence of water on slope stability is also investigated, and the influence of the membership function on the results is also discussed. The end is the conclusion drawn by this study.

2 Method

2.1 Failure Probabilities Calculation Involving Limit-State Function's Ambiguity

A limit-state function (F) for side-slope stability analysis was often written as [5]:

$$F = F_s - 1 \tag{1}$$

In the above equation, F_s represents the slope safety factor, which can be calculated using methods including limit equilibrium theory. When $F > 0$, slopes are considered to be in a safe domain; when $F \leq 0$, slopes are considered to be in failed domain. There are many factors affecting the safety factor of slope. Besides the mechanical properties of slope soil, water is also an important factor [22–25].

It can be seen from the definition of Eq. (1) that $F_s = 1$ is the strict boundary between slope safety domain and failure domain. However, in practice, when the slope F_s is less than 1, it also may not be unstability, and when it is greater than 1, the slope may not be safe. This shows that there is also an intermediate region between the safety and unsafety regions of slopes, which can be both unstability and safe. That is, limit-state functions for slopes are fuzzy, which can be characterized by a fuzzy membership function [26]. Combining fuzzy membership theory, the fuzzy membership for the limit-state function for slope stability is:

$$u(F) = \begin{cases} 1, & F \geq b \\ \dfrac{F-a}{b-a}, & a < F < b \\ 0, & F \leq a \end{cases} \tag{2}$$

In Eq. (2), a and b represent two parameters. In this paper, we set $b = 0.5$, $a = -0.5$. That is, if slope F_s is larger than 1.5, one can determine that this slope is in a safe state, and when the slope safety factor is less than 0.5, the slope is considered to be unstable. Slopes with a safety factor between 0.5 and 1.5 are likely to be unstable, and the probability of instability decreases as the slope safety factor increases [17]. According to the form of Eq. (2), Eq. (1) can be rewritten as:

$$u(F) = \begin{cases} 1, F > 0 \\ 0, F \leq 0 \end{cases} \tag{3}$$

Fig. 2 shows the comparison of Eqs. (2) and (3). Failure probability (P_f) could obtained according to Eq. (4):

$$P_f = 1 - \frac{1}{N}\sum_{i=1}^{N} u(F) \tag{4}$$

In the equation, N is the number of sampling points. By substituting Eq. (2) into Eq. (4), a failure probability considering limit-state function ambiguity can be calculated, and by substituting Eq. (3) into Eq. (4), a failure probability without considering limit-state ambiguity can be obtained. It can be seen from Eqs. (2) and (3) that when $a = b = 0$, the method of considering limit-state ambiguity will degenerate into the method of not considering limit-state ambiguity.

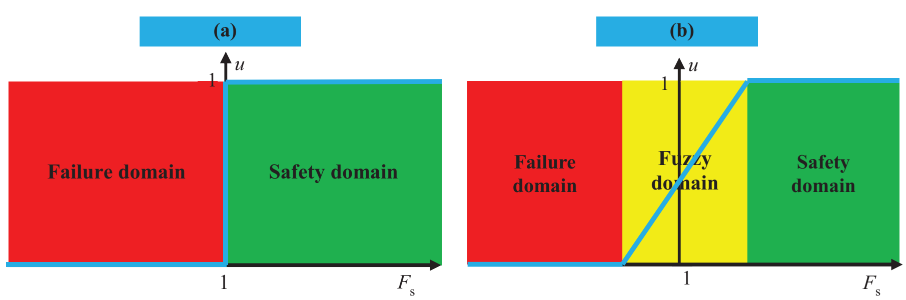

Figure 2: Calculation of membership: (a) without considering the fuzzification of the limit-state, and (b) considering the fuzzification of limit-state function

The steps for calculating the slope P_f according to the Monte Carlo method are:

1) Sampling, with a total number of N;

2) Calculate u according to Eq. (2);

3) Calculate the failure probability according to Eq. (3).

When F_s expressed by a simple explicit function, P_f can be calculated directly based on the MCS method. When F_s needs to be calculated by a complex implicit iterative procedure, it is extremely time-consuming to directly calculate the failure probability according to the above method. In view of this, a new model is designed below to replace the limit-state function.

2.2 Alternative Model for Limit-States

An LSSVM optimized by the GWO and K-fold CV algorithm is implemented to replace a limit-state function.

2.2.1 GWO

GWO, as a new swarm-intelligence algorithm, simulates the hunting process of grey wolves [19]. In this section, we briefly introduce the basic process of GWO.

In GWO, all wolves are divided into four categories (alpha wolves, beta wolves, delta wolves, and omega wolves), and the first three categories guide the behavior of the last one. The process of wolves surrounding the prey is described as follows [19]:

$$X_{t+1} = X_{p,t} - \mu \cdot d \tag{5}$$

$$d = \left| c \cdot X_{p,t} - X_t \right| \tag{6}$$

$$\mu = 2 \cdot b \cdot rand_1 - b \tag{7}$$

$$c = 2 \cdot rand_2 \tag{8}$$

where X_{t+1} represents a location of a wolf at (t+1)th iteration, and X_t represents a wolf's location at tth iteration, and $X_{p,t}$ represents the prey's location at tth iteration. During the iteration, b linearly reduces from 2 to 0 [19]. The grey wolves hunting process is modeled as follows:

$$X_1' = X_\alpha - \mu_\alpha \cdot d_\alpha \tag{9}$$

$$X_2' = X_\beta - \mu_\beta \cdot d_\beta \tag{10}$$

$$X_3' = X_\delta - \mu_\delta \cdot d_\delta \tag{11}$$

$$X_{t+1} = \left(X_1' + X_2' + X_3' \right) / 3 \tag{12}$$

In the equation, X_α, X_β, and X_δ are respectively the best guide, second-best guide, and third-best guide. Eqs. (5)–(12) constitute the core of GWO. Unlike the Particle Swarm Optimization [27], which requires the user to specify multiple parameters, there are only two parameters that need to be specified by the user in GWO, i.e., population size and the total iterations.

2.2.2 LSSVM

SVM transforms vectors in an input space to a new feature space using a nonlinear rule, and then converts the actual problem into a quadratic programming problem with inequality constraints. LSSVM is an extension of SVM. LSSVM replaces the inequality constraints in SVM with equality constraints and adopts a squared-error loss function as the training set's empirical loss, thereby transforming the primary problem into a linear matrix solution problem [18].

The model expression of LSSVM is:

$$f(\boldsymbol{x}) = \boldsymbol{w}^{\mathrm{T}}\varphi(\boldsymbol{x}) + b \tag{13}$$

in which, x represents input matrix, wand b are parameters, φ is a nonlinear function.

The parameter w in Eq. (13) is:

$$\boldsymbol{w} = \sum_{i=1}^{m} \lambda_i \varphi(x_i) \tag{14}$$

in which, λ_i is Lagrange multiplier, m is sample total number.

According to Eqs. (14) and (13), we have:

$$f(\boldsymbol{x}) = \sum_{i=1}^{m} \lambda_i \varphi(x_i)^T \varphi(\boldsymbol{x}) + b \tag{15}$$

and Eq. (15) can also be written as:

$$f(\boldsymbol{x}) = \sum_{i=1}^{m} \lambda_i K(x_i, \boldsymbol{x}) + b \tag{16}$$

In which, K is a kernel function. This paper chooses a gaussian function, defined as follows:

$$K(x_i, \boldsymbol{x}) = \exp\left\{-\|\boldsymbol{x} - \boldsymbol{x_i}\| \big/ \boldsymbol{2\sigma^2}\right\} \tag{17}$$

λ_{i} and b need to be obtained througth a linear equation:

$$\begin{bmatrix} 0 & \mathbf{1}^T \\ \mathbf{1} & K(x_i, \boldsymbol{x}) + C^{-1}\boldsymbol{I} \end{bmatrix} \begin{bmatrix} b \\ \boldsymbol{\lambda} \end{bmatrix} = \begin{bmatrix} 0 \\ \boldsymbol{y} \end{bmatrix} \tag{18}$$

where $\mathbf{1} = [1, 1, \ldots, 1]_{m\times 1}$, $\boldsymbol{\lambda} = [\lambda_1, \lambda_2, \ldots, \lambda_m]^T$, $\boldsymbol{y} = [y_1, y_2, \ldots, y_m]^T$. $\boldsymbol{I} = 1_{m\times m}$, and y are output vectors, C represents a penalty factor.

σ in Eq. (17) and C in Eq. (18) are hyperparameters. They can be solved by GWO. The objective function (fitness) of GWO is set to:

$$fitness = \sqrt{(f(\boldsymbol{x}) - \boldsymbol{y})^2} \Big/ m \tag{19}$$

Eq. (19) is also called root mean square error (RMSE) function.

When hyperparameters are determined, a K-fold CV algorithm is also performed to divide samples (in Section 3 of this article, K = 5), which is a training method to improve generalization abilityof machine learning.

To better explain the proposed method, Fig. 3 gives a flowchart of calculation method of failure probability proposed in this paper. The following will use 3 examples to verify our method.

It is noted that water is the main factor influencing the stability of slopes. Thus, in the calculation of the safety factor in Eqs. (1)–(4), the effect of water should be incorporated. In this paper, the impact of water on slopes is analyzed through fluid dynamics. Specifically, it is reflected by calculating the phreatic line after the change in water level. Fig. 4 presents a simple model for calculating the saturation line, where h_0 represents the initial water level and h_{d} represents the variation of the saturation line.

The differential equation that describes the non-stable motion of diving can be expressed as follows [5]:

$$\frac{\partial h_{\mathrm{d}}}{\partial t} = a \frac{\partial^2 h_{\mathrm{d}}}{\partial x^2} \tag{20}$$

where x and t denote the position and time of the calculation point, respectively; a is a coefficient related to the coefficient of permeability. The solution of Eq. (20) can be deduced by Laplace transform, namely:

$$h_{\mathrm{d}} = v_0 t M\left(x/2\sqrt{at}\right) \tag{21}$$

v_0 indicates the rate of water level drop, while M is a sign function, that is:

$$M(x) = 0.1091x^4 - 0.7501x^3 + 1.9283x^2 - 2.2319x + 1 \tag{22}$$

Based on Fig. 4, the coordinate h of the saturation line can be represented as:

$$h = h_0 - h_{\mathrm{d}} \tag{23}$$

Based on Eqs. (20)–(23), the phreatic line can be determined. Once the phreatic line is determined, the unit weight of the soil above the line is taken as the natural unit weight, and the unit weight below the line is taken as the saturated unit weight.

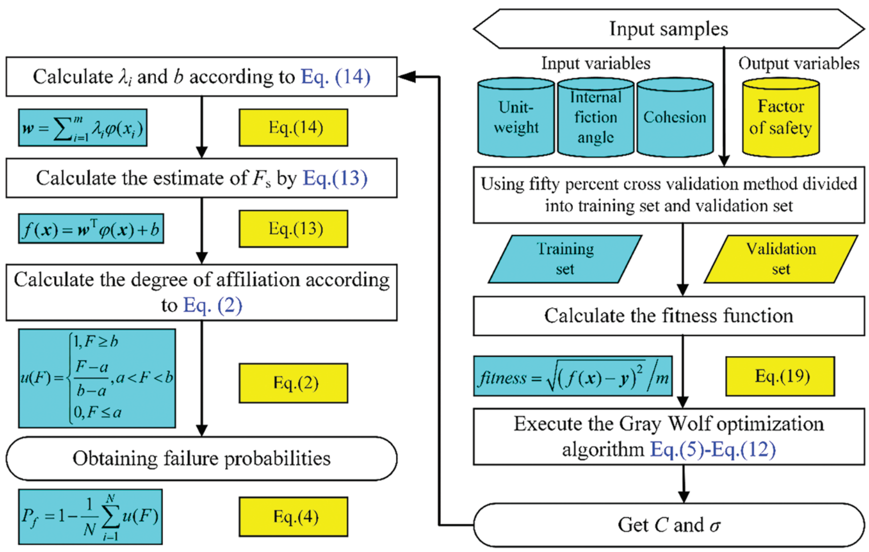

Figure 3: Calculation flow chart of the proposed method

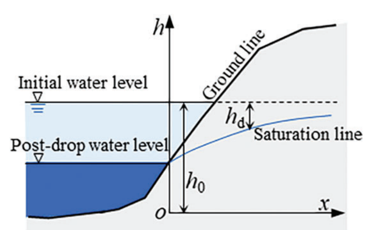

Figure 4: A simplified model for calculating the saturation line

3 Results and Discussion

It is worth noting that all the following calculations are done by MATLAB 2018a on a computer with a Windows 10 system. Fig. 5 shows the iteration curves of the Grey Wolf Optimizer (GWO) for three different slope stability analysis cases (1D, 2D, and 3D slopes). The x-axis represents the number of iterations, and the y-axis indicates the fitness value. Each subfigure (a), (b), and (c) corresponds to Case 1 (1D slope), Case 2

(2D slope), and Case 3 (3D slope), respectively. Fig. 5a depicts the convergence of GWO for the 1D slope is achieved within approximately 20 iterations, indicating efficient optimization. Fig. 5b depicts the iteration curve for the 2D slope, showing similar convergence behavior, reaching the optimum around the 20th iteration. Fig. 5c depicts the iteration curve for the 3D slope, with convergence occurring around the 30th iteration, reflecting the increased complexity of the model.

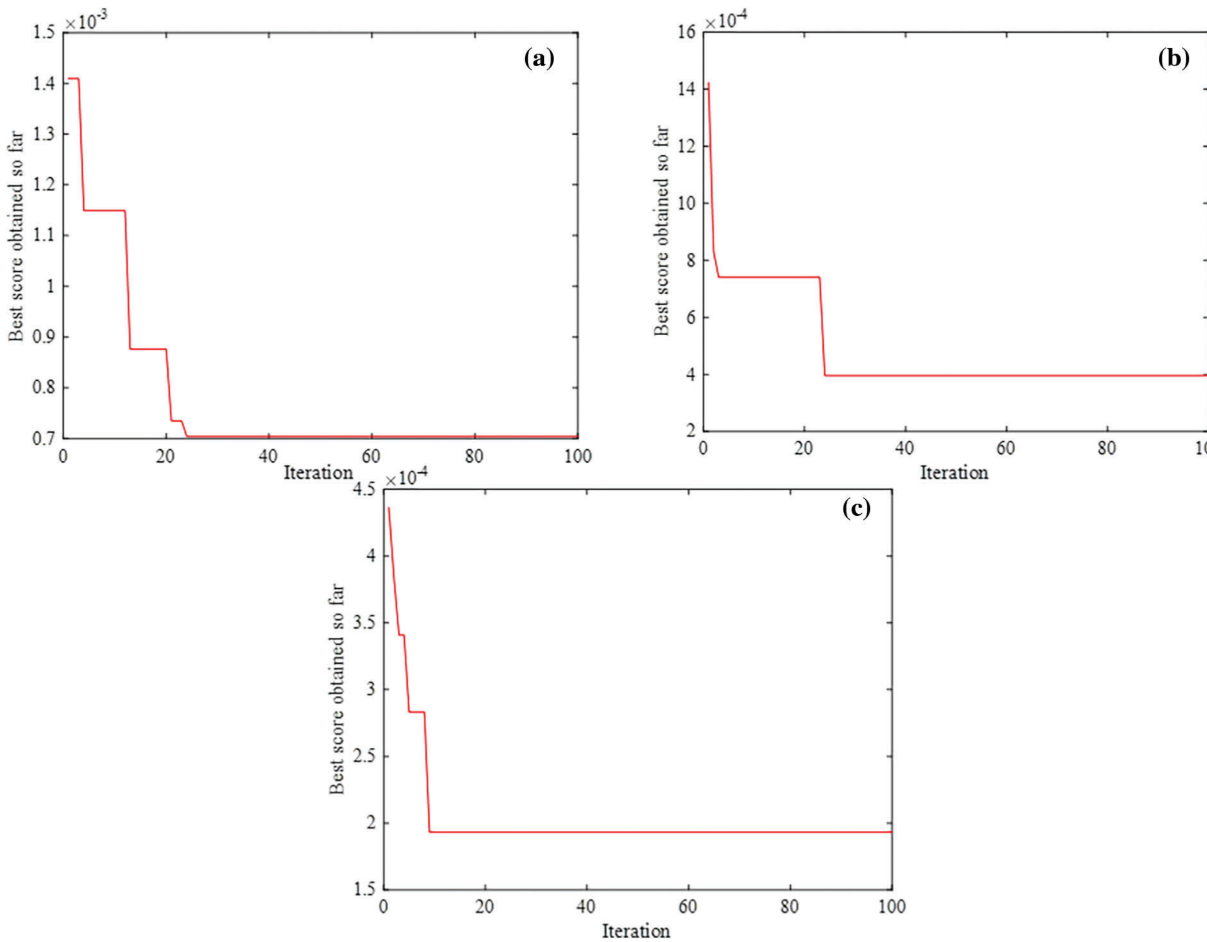

Figure 5: Iteration curve of GWO: (a) Case one, (b) Case two, (c) Case three

3.1 Results

3.1.1 Case 1

Case 1 is a 1D slope (Fig. 6). On the 1D slope, the slip surface is a straight line. The slope gradient is 30°. The soil's weight, cohesion, and friction coefficient are uncertain parameters that satisfy the normal distribution (Table 1). The safety factor F_s of the 1D slope is calculated using the following equation:

$$F_s = \frac{(2(\mathit{Unit\ weight})\cos^2 30^\circ)\tan(\text{Internal friction angle}) + \text{Cohesion}}{2(\mathit{Unit\ weight})\cos 30^\circ \sin 30^\circ} \tag{24}$$

One hundred samples are generated, and the values of C and σ are obtained according to the method in Fig. 3, as shown in Table 2. Among them, the population size and total iterations of GWO are set to 20 and 100, respectively. Fig. 5a shows the iteration curve of GWO. It can be seen that after about 20 generations, GWO tends toward the global optimal value. By setting the sampling times to 30,000, the P_f for this slope is find to be 0.072%. MCS is the most accurate method to calculate the failure probability of landslide. By MCS method, P_f is 0.074%, and the relative deviation between the two is only 2.34%.

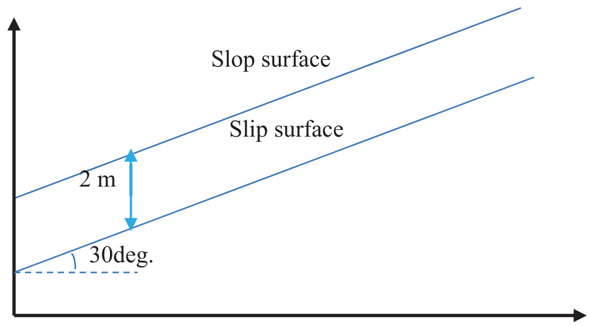

$$F_s = \frac{(2(Unit\ weight)\cos^2 30^\circ)\tan(\text{Internal friction angle}) + \text{Cohesion}}{2(Unit\ weight)\cos 30^\circ \sin 30^\circ}$$

Figure 6: One-dimensional slope

Table 1: Distribution form and numerical characteristics of uncertain parameters

Cases	Properties	Means	Standard deviations	Distribution type
1	Unit-weight (kN/m^3)	18.60	0.93	Normal
	Cohesion (kPa)	22.70	3.41	Normal
	Internal friction angle (deg.)	20.00	3.00	Normal
2	Unit weight (kN/m^3)	18.60	0.93	Normal
	Cohesion (kPa)	25.00	3.75	Normal
	Internal friction angle (deg.)	23.00	3.45	Normal
3	Unit weight (kN/m^3)	20.60	1.03	Normal
	Cohesion (kPa)	26.70	4.01	Normal
	Internal friction angle (deg.)	25.00	3.75	Normal

Table 2: LSSVM parameters

Cases	C	σ
1	2139.33	94.80
2	3529.90	190.15
3	3715.75	307.82

3.1.2 Case 2

Case 2 is a 2D slope (Fig. 7). On the 2D slope, the slip surface is a curve. In this example, there are three types of normal distributions: the first one is for severity with a mean of 18.60 and a standard deviation of 0.93; the second one is for cohesion with a mean of 25.00 and a standard deviation of 3.75; the third one is for friction angle with a mean of 23.00 and a standard deviation of 3.45. The safety factor for this slope was calculated using the MP method [28]. One hundred samples are generated (Table 3), and the values of C and σ are obtained according to the method in Fig. 3 as shown in Table 2. Fig. 5b shows the iteration curve of GWO. It can be seen that after about 20 generations, GWO tends toward the global optimal value. By setting the sampling times to 30,000 times, a P_f of 2.518% can be obtained. The P_f obtained by MCS method is 2.58%, and the relative deviation between the two is only 2.48%.

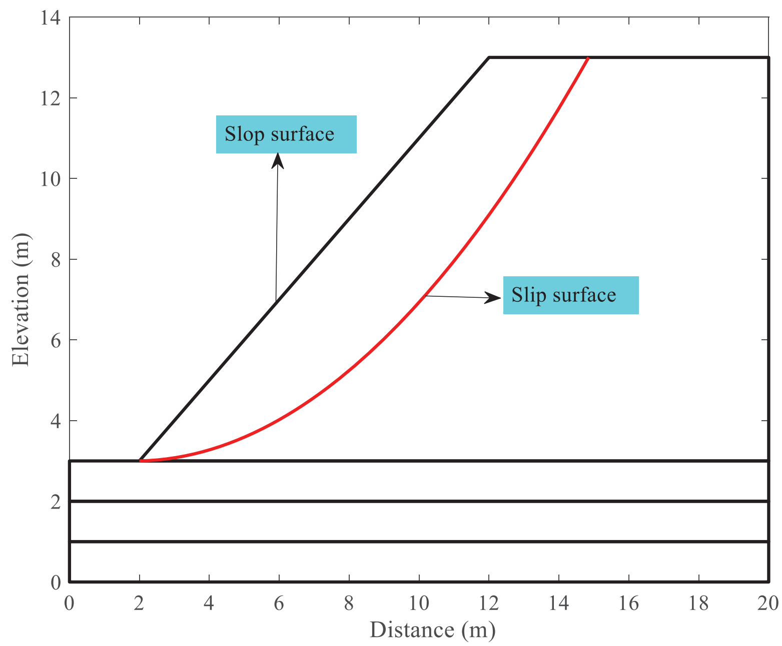

Figure 7: Two-dimensional slope

Table 3: Calculation samples for Case 2 (F_s is calculated according to MP method)

No.	Unit weights (kN/m^3)	Cohesion (kPa)	Internal friction angles (deg.)	F_s	No.	Unit weights (kN/m^3)	Cohesion (kPa)	Internal friction angles (deg.)	F_s
1	17.463	26.162	19.046	1.653	51	16.880	24.722	18.563	1.613
2	18.008	21.862	23.034	1.542	52	16.412	17.350	25.673	1.496
3	20.601	32.323	20.114	1.737	53	19.141	30.241	24.330	1.866
4	17.433	28.375	22.099	1.839	54	20.115	25.735	23.735	1.613
5	18.776	30.675	17.410	1.714	55	19.593	18.316	28.602	1.490
6	19.569	20.620	24.532	1.460	56	19.407	29.754	21.272	1.742
7	19.479	29.484	17.346	1.619	57	18.134	21.279	16.866	1.340
8	18.395	22.522	18.251	1.417	58	18.099	29.712	21.672	1.838
9	18.871	29.836	23.580	1.845	59	18.813	25.840	20.917	1.607
10	20.018	24.936	24.271	1.602	60	21.092	22.721	20.458	1.362
11	18.824	23.975	22.993	1.587	61	18.041	21.477	26.626	1.629
12	19.388	29.370	18.916	1.662	62	17.742	24.184	23.172	1.662
13	17.471	20.962	26.696	1.638	63	18.874	27.061	27.094	1.834

(Continued)

Table 3 (continued)

No.	Unit weights (kN/m^3)	Cohesion (kPa)	Internal friction angles (deg.)	F_s	No.	Unit weights (kN/m^3)	Cohesion (kPa)	Internal friction angles (deg.)	F_s
14	20.497	29.292	23.775	1.731	64	18.166	26.823	26.724	1.856
15	19.321	31.462	28.252	2.022	65	18.652	20.363	23.991	1.474
16	18.411	19.967	22.363	1.421	66	17.281	22.038	20.700	1.524
17	18.527	20.517	24.306	1.495	67	18.622	27.252	30.792	1.974
18	20.690	19.960	18.996	1.234	68	20.077	28.959	21.359	1.673
19	17.080	21.946	23.856	1.621	69	18.598	27.243	20.813	1.675
20	19.355	23.340	26.623	1.641	70	19.271	27.762	22.317	1.699
21	19.853	25.861	26.153	1.703	71	18.650	24.222	27.085	1.728
22	20.150	18.307	23.694	1.321	72	19.350	23.816	20.968	1.496
23	18.171	26.411	21.234	1.678	73	17.947	25.468	22.326	1.682
24	18.384	25.242	19.690	1.572	74	20.098	23.115	13.943	1.245
25	18.816	21.086	26.135	1.559	75	17.672	16.663	21.898	1.297
26	19.227	25.980	27.098	1.769	76	17.961	22.385	26.000	1.654
27	19.972	26.634	26.108	1.725	77	20.374	22.814	18.269	1.336
28	18.106	25.091	17.861	1.533	78	19.370	24.809	17.778	1.448
29	18.346	25.899	27.572	1.831	79	17.113	28.878	20.169	1.831
30	20.417	37.310	19.161	1.913	80	17.641	23.212	22.966	1.619
31	17.937	30.049	31.342	2.158	81	19.273	26.721	24.760	1.727
32	18.871	24.897	22.625	1.612	82	20.471	25.942	24.997	1.640
33	16.796	24.533	26.243	1.829	83	19.845	26.893	28.346	1.811
34	18.613	24.568	23.327	1.633	84	19.017	29.138	26.830	1.903
35	18.121	20.426	23.915	1.499	85	18.894	20.599	22.414	1.427
36	19.637	26.334	19.053	1.530	86	18.402	23.959	22.014	1.581
37	19.310	25.520	20.449	1.553	87	20.058	23.912	21.314	1.476
38	19.728	21.201	22.639	1.421	88	17.392	23.281	23.066	1.640
39	19.206	36.425	25.933	2.161	89	18.957	28.936	16.752	1.613
40	18.618	26.391	17.149	1.538	90	16.644	22.879	23.087	1.669
41	17.900	34.405	25.436	2.166	91	19.204	27.627	25.309	1.784
42	18.237	31.254	26.938	2.048	92	18.404	26.167	31.311	1.959
43	19.759	25.474	21.490	1.557	93	19.883	23.505	18.388	1.388
44	19.309	19.419	25.678	1.456	94	17.166	26.388	22.766	1.787
45	17.737	22.105	25.766	1.647	95	20.152	27.757	23.241	1.675
46	17.885	28.484	24.443	1.879	96	18.565	27.452	23.298	1.756
47	20.931	20.571	21.642	1.321	97	18.045	24.720	16.219	1.477
48	18.099	21.357	27.442	1.646	98	18.228	23.842	30.615	1.847

(Continued)

Table 3 (continued)

No.	Unit weights (kN/m^3)	Cohesion (kPa)	Internal friction angles (deg.)	F_s	No.	Unit weights (kN/m^3)	Cohesion (kPa)	Internal friction angles (deg.)	F_s
49	18.747	29.616	15.960	1.633	99	17.262	22.907	30.071	1.844
50	18.369	24.569	22.805	1.632	100	18.518	22.192	25.461	1.600

3.1.3 Case 3

Case 3 is a 3D slope (Fig. 8). In the 3D slope, the slip surface is a curved surface. The slope gradient is 45°. Fig. 8 provides a schematic of a three-dimensional slope used in the case study. This figure illustrates the complex geometry of the 3D slope, including the weight stress and normal stress acting on the slope. In this example, the severity has a mean of 20.60 and a standard deviation of 1.03, the cohesion has a mean of 26.70 and a standard deviation of 4.01, and the internal friction angle has a mean of 25.00 and a standard deviation of 3.75. The safety factor F_s of a 3D slope was calculated using a direct stress [29] approach. As shown in Fig. 8, the method makes it possible for us to obtain F_s by solving the Eq. and adjusting the self-weight stress. The samples used to train the LSSVM are shown in Table 4. Similar to the above two examples, the values of C and σ are 3715.75 and 307.82, respectively. GWO also toward the global optimal solution after 10 iterations. By setting the sampling times to 30,000, the failure probability of this slope is found to be 38.320%. The P_f obtained by MCS method is 37.8%, and the relative deviation between the two is 1.35%.

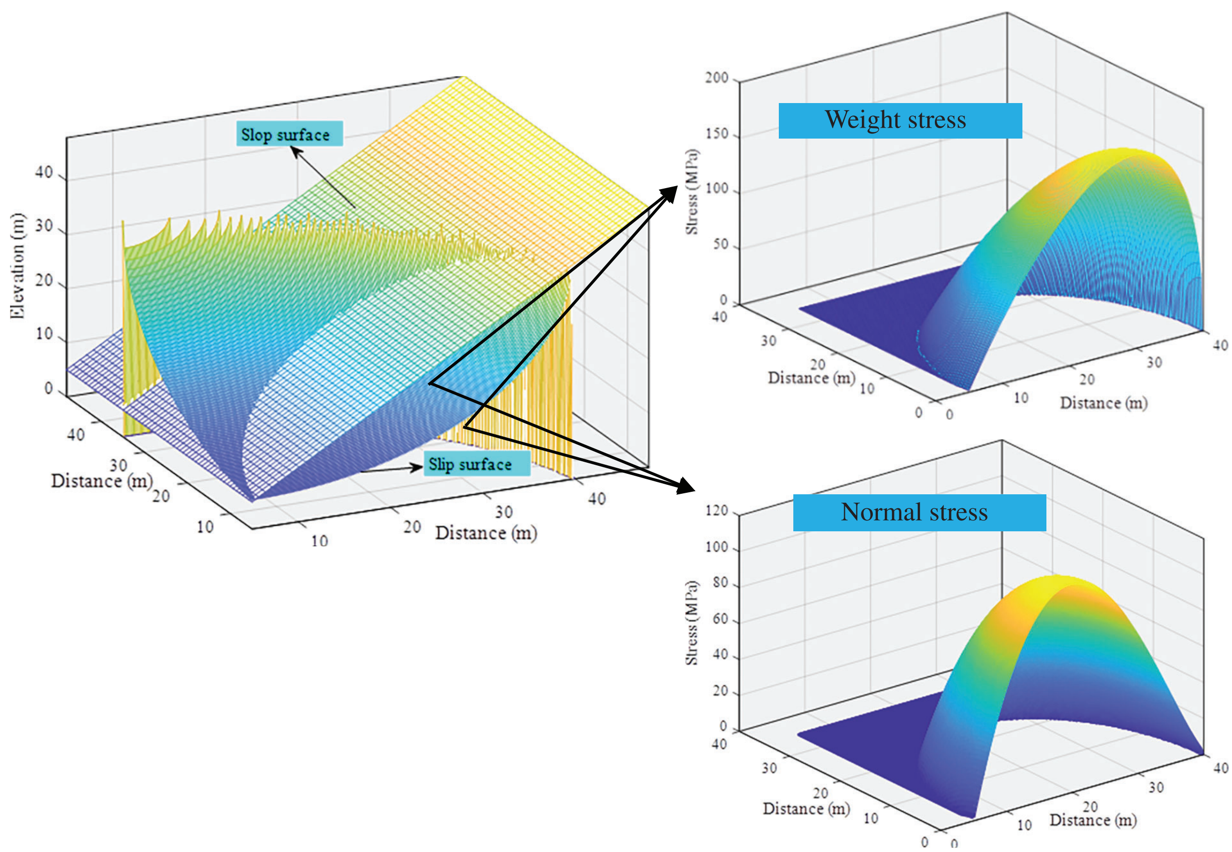

Figure 8: Three-dimensional slope

Table 4: Calculation samples for Case 3 (F_s is calculated according to the normal stress method)

No.	Unit weights (kN/m^3)	Cohesions (kPa)	Friction angles (deg.)	F_s	No.	Unit weights (kN/m^3)	Cohesions (kPa)	Friction angles (deg.)	F_s
1	19.450	25.080	28.615	1.228	51	20.286	23.198	28.704	1.183
2	21.426	25.040	20.752	0.943	52	20.175	25.692	25.992	1.137
3	20.604	25.449	23.505	1.047	53	21.399	32.365	23.228	1.130
4	19.907	28.137	27.617	1.235	54	20.905	28.778	23.569	1.095
5	21.333	27.368	19.157	0.934	55	21.604	17.293	25.406	0.964
6	19.497	19.143	25.228	1.017	56	20.434	22.844	28.789	1.177
7	18.709	17.611	19.481	0.831	57	20.578	25.590	22.806	1.028
8	20.760	25.776	26.902	1.156	58	20.167	30.848	25.951	1.220
9	21.264	25.621	24.347	1.063	59	19.788	26.048	22.954	1.057
10	20.373	21.274	25.689	1.052	60	19.522	26.857	31.345	1.350
11	21.808	29.328	25.924	1.158	61	21.150	30.407	28.941	1.287
12	20.372	24.843	29.845	1.246	62	20.810	25.411	26.829	1.147
13	20.542	30.651	25.201	1.184	63	19.629	22.830	23.344	1.018
14	19.617	25.832	19.109	0.944	64	19.335	26.312	22.037	1.044
15	19.519	30.707	22.885	1.140	65	20.566	26.825	28.974	1.245
16	20.671	25.133	22.759	1.018	66	20.665	17.898	29.528	1.121
17	19.451	26.949	24.312	1.121	67	19.982	24.010	18.579	0.891
18	21.166	27.647	23.487	1.070	68	19.186	26.577	20.610	1.010
19	21.559	25.483	24.662	1.065	69	19.600	21.056	19.659	0.880
20	19.564	32.348	19.464	1.066	70	20.271	24.131	24.696	1.069
21	21.379	28.224	23.975	1.089	71	21.913	28.903	22.571	1.046
22	18.180	21.237	20.297	0.929	72	22.125	29.338	23.081	1.064
23	19.557	31.038	28.692	1.328	73	19.504	26.831	27.588	1.222
24	20.494	22.485	29.238	1.186	74	20.792	22.018	20.198	0.890
25	21.872	33.741	24.559	1.181	75	20.442	18.093	24.588	0.966
26	22.129	32.376	21.470	1.061	76	22.084	26.487	19.761	0.924
27	19.078	26.637	36.945	1.568	77	22.106	25.186	20.531	0.926
28	21.963	23.172	25.106	1.037	78	21.051	21.485	26.841	1.081
29	18.806	23.294	23.430	1.046	79	20.883	30.996	18.189	0.974
30	19.415	29.149	23.576	1.137	80	22.072	31.302	24.157	1.127
31	20.460	28.073	23.316	1.086	81	20.470	25.990	28.659	1.223
32	20.416	27.325	21.243	1.013	82	18.969	27.322	31.375	1.372
33	21.007	30.437	28.168	1.265	83	20.884	27.018	26.109	1.147

(Continued)

Table 4 (continued)

No.	Unit weights (kN/m^3)	Cohesions (kPa)	Friction angles (deg.)	F_s	No.	Unit weights (kN/m^3)	Cohesions (kPa)	Friction angles (deg.)	F_s
34	20.278	29.441	25.779	1.189	84	19.808	30.393	28.646	1.309
35	21.466	21.628	26.624	1.070	85	21.498	25.770	28.939	1.209
36	22.289	19.228	26.556	1.021	86	22.140	24.728	23.610	1.011
37	22.187	25.630	28.086	1.166	87	18.752	20.173	17.147	0.809
38	21.777	19.298	22.501	0.902	88	19.834	29.074	30.087	1.335
39	21.976	20.895	26.417	1.045	89	19.880	26.325	24.634	1.111
40	22.363	32.085	21.743	1.060	90	20.929	24.291	23.714	1.029
41	20.021	24.699	29.885	1.252	91	20.697	27.789	24.577	1.115
42	20.341	31.849	16.580	0.956	92	19.970	24.894	30.203	1.268
43	21.346	19.142	22.522	0.906	93	21.095	26.300	24.362	1.077
44	20.401	27.298	33.162	1.403	94	21.283	25.638	20.262	0.940
45	20.300	27.389	22.146	1.043	95	21.102	32.787	26.012	1.230
46	21.421	23.426	27.822	1.137	96	20.271	27.057	17.762	0.912
47	18.676	28.303	29.120	1.319	97	18.845	33.769	19.873	1.124
48	19.461	25.808	25.921	1.152	98	21.016	25.175	24.540	1.066
49	20.411	28.933	27.693	1.239	99	21.053	24.499	30.364	1.246
50	18.305	25.676	26.798	1.205	100	20.996	26.479	31.151	1.305

Water constitutes one of the crucial factors influencing slope stability. Consequently, the proposed methodology is employed to analyze the failure probability of the three slopes under water-immersed conditions (refer to Eqs. (20)–(23)).

Table 5 presents the outcomes of the three slopes under water-immersed conditions. In three cases, a = 30, v_0 = 0.2 m/day, and t = 360 days. It can be observed that for Case 1, the failure probability of the slope under water-immersed condition amounts to 0.09%, which is 25% higher than that under the natural condition. For Case 2, the failure probability of the slope under water-immersed condition is 3.198%, which is 27% higher than that under the natural condition. For Case 3, the failure probability of the slope under water-immersed condition is 50.199%, which is 31% higher than that under the natural condition.

Table 5: Failure probability under wading condition

Cases	P_f
1	0.090
2	3.198
3	50.199

3.2 Discussion

3.2.1 Accuracy and Calculation Time

An exact solution for slope failure probability can be acquired through the MCS method. After 30,000 times of sampling, the failure probabilities of the slopes in Cases 1–3 were 0.074%, 2.582%, and 37.810%, respectively. The errors of the proposed method in comparison with the MCS method are 2.341841%, 2.478699%, and 1.34885% (Table 6). As can be observed, the proposed method possesses high accuracy and can satisfy the requirements of engineering applications.

Table 6: Comparison of our approach with MCS

Cases	MCS	Proposed method	Error (%)
1	0.074	0.072	2.341841
2	2.582	2.518	2.478699
3	37.810	38.320	1.34885

Fig. 9 compares the computation time required for the proposed LSSVM-GWO method and the MCS method across the three case studies (1D, 2D, and 3D slopes). The x-axis represents the different cases, while the y-axis indicates the computation time in seconds. In Cases 1–3, the calculation times of our proposed method are 31.45, 29.17, and 30.33 s, while the times for the MCS method are 0.02, 5260.75, and 83114.99 s (Fig. 9). Except for the 1D slope, our method takes much less time than the MCS algorithm. Since the F_s expression of the 1D slope can be expressed using a simple explicit function, it only takes a short time to calculate P_f directly according to the MCS approach. However, calculation according to the MCS method for 2D and 3D slopes requires much more time. The calculation complexity of the safety factor for 1D to 3D slopes gradually increases. In the calculation of P_f for 2D and 3D slopes, the MCS approach takes 180 times and 2740 times longer than our approach, respectively. The calculation time of our approach is not affected by the complexity of the safety factor model and averages about 30 s. The proposed method has significant advantages over the MCS method in calculating the failure probability of complex slopes.

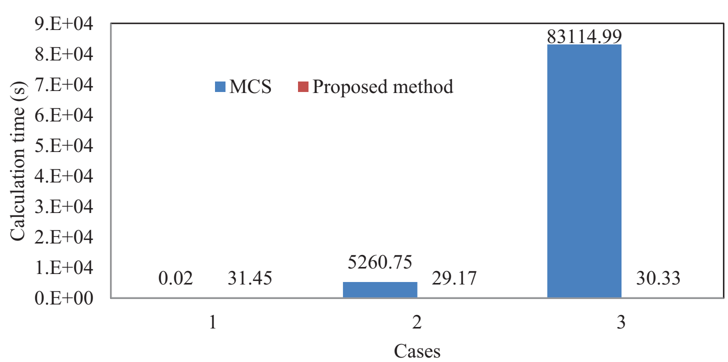

Figure 9: Comparing the calculation time of this method with the strict MCS method

3.2.2 Comparison of Proposed and Probabilistic Methods

Here, we call the method that does not consider the function of the limit-state a Probabilistic method. Our approach considers the ambiguity of limit-state. Table 3 compares differences between the calculation results of the two. Fig. 10 presents the failure probability results obtained using the proposed LSSVM-GWO method and the classical probabilistic method. The x-axis represents the different cases

(1D, 2D, and 3D slopes), while the y-axis indicates the failure probability percentage. According to Probabilistic method, samples were sampled 30,000 times, and the failure probabilities were 0%, 0.040% and 19.550% (Fig. 10). Probabilistic approach is quite different from the proposed approach. In comparison, the probabilistic method underestimates the failure probability of the slope.

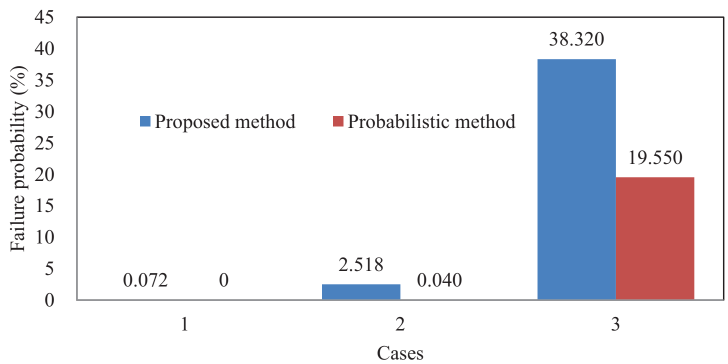

Figure 10: Calculation results of the present approach and probabilistic method

3.2.3 Comparison of Different Membership Functions

Except for linear membership rule used in Eq. (2), in fuzzy field, the common membership functions are normal type and Cauchy type [30].

$$u(F) = \begin{cases} 1, & F \geq b \\ \exp\left(-\dfrac{(F-b)^2}{b}\right), & F < b \end{cases} \tag{25}$$

$$u(F) = \begin{cases} 1, & F \geq b \\ \dfrac{b}{b+10(F-b)^2}, & F < b \end{cases} \tag{26}$$

Fig. 11 compares P_f calculation results of the above membership functions used in three cases. The parameter settings are the same as in Section 3.1. As shown in Fig. 11 the difference in the failure probability of several membership functions is relatively small. In contrast, P_f determined by normal membership function is less than the linear function, and P_f by Cauchy membership function is greater than the linear membership function. In practice, using linear membership function is a compromise.

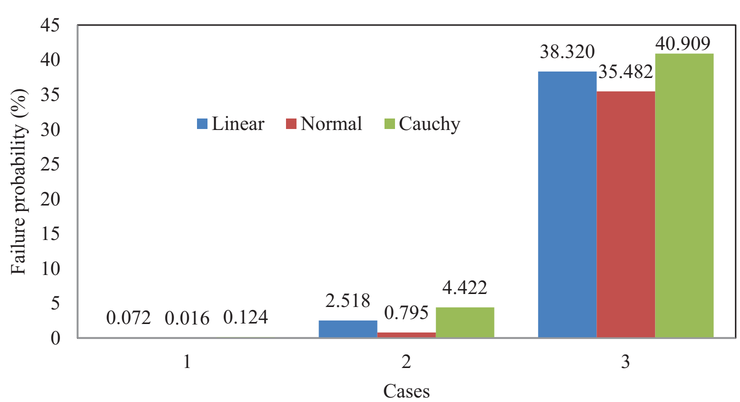

Figure 11: Comparison of different membership functions

4 Conclusions

This study introduces a novel approach for calculating slope failure probability by incorporating the ambiguity of the limit-state function. The developed method leverages a Least Squares Support Vector Machine (LSSVM) optimized by the Grey Wolf Optimizer (GWO) and K-fold cross-validation to replace traditional limit-state function methods, significantly reducing computational time while maintaining high accuracy.

1. The proposed method was tested on three cases: one-dimensional (1D), two-dimensional (2D), and three-dimensional (3D) slopes. The results demonstrate that the accuracy of our algorithm is exceptional, with an error margin within 3% compared to the strict Monte Carlo Simulation (MCS) method. This accuracy is sufficient to meet engineering requirements, indicating that the alternative model method established in this study is highly reliable and accurate for practical applications. For 1D, 2D and 3D conditions, the probability of failure under wading conditions is 25%, 27%, and 31% higher than that under natural conditions, respectively.
2. One of the significant advantages of the proposed method is its efficiency in reducing computational time, especially for complex limit-state functions. In the calculation of 2D and 3D slope failure probabilities, the proposed method is approximately 180 times and 2740 times faster than the MCS method, respectively. This dramatic reduction in computation time highlights the method's potential for real-time applications and large-scale simulations where traditional methods would be impractical due to time constraints.
3. Compared with our algorithm, the classical probabilistic methods tend to underestimate the slope failure probability. This disparity highlights the significance of considering the ambiguity in the limit-state function, which our method effectively handles. The incorporation of this ambiguity offers a more realistic and precise estimation of slope failure probabilities, rendering the proposed method superior in scenarios where precision is of vital importance.
4. The type of membership function used in the fuzzy limit-state model significantly influences the calculated failure probability. Our findings show that the failure probability obtained using a linear membership function lies between those derived from normal and Cauchy membership functions. This sensitivity to membership function types suggests that careful selection and tuning of these functions are essential for accurate failure probability estimation.
5. While incorporating the ambiguity from the limit-state function, the method also introduces uncertainty due to human factors, such as the distribution type and parameters of the membership function. This aspect adds a layer of complexity to the analysis but also aligns more closely with real-world conditions where human judgment and variability play a role.

Acknowledgement: The authors gratefully acknowledge the support of Sichuan Hongye Construction Software Co., Ltd. The authors also thank Shaohong Li for his guidance on the calculation method.

Funding Statement: Ministry of Education, Center for Scientific Research and Development of Higher Education Institutions "Innovative Application of Virtual Simulation Technology in Vocational Education Teaching" Special Project, Project No. ZJXF2022110.

Author Contributions: The authors confirm contribution to the paper as follows: study conception and design: Jianing Hao; data collection: Dan Yang; analysis and interpretation of results: Guanxiong Ren, Ying Zhao; draft manuscript preparation: Jianing Hao, Rangling Cao. All authors reviewed the results and approved the final version of the manuscript.

Availability of Data and Materials: The data involved in this study has been provided in the paper.

Ethics Approval: Not applicable.

Conflicts of Interest: The authors declare no conflicts of interest to report regarding the present study.

References

1. Robson E, Milledge D, Utili S, Dattola G. A computationally efficient method to determine the probability of rainfall-triggered cut slope failure accounting for upslope hydrological conditions. Rock Mech Rock Eng. 2022;57(4):2421–43.
2. Gupta K, Satyam N, Gupta V. Probabilistic physical modelling and prediction of regional seismic landslide hazard in Uttarakhand state (India). Landslides. 2023;20(5):901–12. doi:10.1007/s10346-022-02013-3.
3. Deng J, Pandey M. Optimal maximum entropy quantile function for fractional probability weighted moments and its applications in reliability analysis. Appl Math Model. 2023;114:230–51. doi:10.1016/j.apm.2022.10.004.
4. Zeng P, Li T, Jimenez R, Feng X, Chen Y. Extension of quasi-Newton approximation-based SORM for series system reliability analysis of geotechnical problems. Eng Comput. 2017;34(2):215–24.
5. Cho SE. Probabilistic stability analyses of slopes using the ANN-based response surface. Comput Geotech. 2017;36(5):787–97.
6. Ling C, Lu Z, Sun B, Wang M. An efficient method combining active learning Kriging and Monte Carlo simulation for profust failure probability. Fuzzy Set Syst. 2020;387:89–107. doi:10.1016/j.fss.2019.02.003.
7. Abad ARB, Ghorbani H, Mohamadian N, Davoodi S, Mehrad M, Aghdam SK, et al. Robust hybrid machine learning algorithms for gas flow rates prediction through wellhead chokes in gas condensate fields. Fuel. 2022;308:121872. doi:10.1016/j.fuel.2021.121872.
8. Nwazelibe VE, Unigwe CO, Egbueri JC. Testing the performances of different fuzzy overlay methods in GIS-based landslide susceptibility mapping of Udi Province, SE Nigeria. CATENA. 2023;220:106654. doi:10.1016/j.catena.2022.106654.
9. Luo Z, Hu B. Robust design of energy piles using a fuzzy set-based point estimate method. Cold Reg Sci Technol. 2019;168:102874. doi:10.1016/j.coldregions.2019.102874.
10. Valdebenito MA, Beer M, Jensen HA, Chen J, Wei P. Fuzzy failure probability estimation applying intervening variables. Struct Saf. 2020;83:101909. doi:10.1016/j.strusafe.2019.101909.
11. Hwang IT, Park HJ, Lee JH. Probabilistic analysis of rainfall-induced shallow landslide susceptibility using a physically based model and the bootstrap method. Landslides. 2023;20(4):829–44. doi:10.1007/s10346-022-02014-2.
12. Shahabi H, Ahmadi R, Alizadeh M, Hashim M, Al-Ansari N, Shirzadi A, et al. Landslide susceptibility mapping in a mountainous area using machine learning algorithms. Remote Sens. 2023;15(12):3112. doi:10.3390/rs15123112.
13. Li H, Nie X. Structural reliability analysis with fuzzy random variables using error principle. Eng Appl Artif Intel. 2018;67:91–9. doi:10.1016/j.engappai.2017.08.015.
14. Ye S, Fang G, Ma X. Reliability analysis of grillage flexible slope supporting structure with anchors considering fuzzy transitional interval and fuzzy randomness of soil parameters. Arab J Sci Eng. 2019;44(10):8849–57. doi:10.1007/s13369-019-03912-9.
15. Wang L, Xiong C, Wang X, Liu G, Shi Q. Sequential optimization and fuzzy reliability analysis for multidisciplinary systems. Struct Multidiscip Optim. 2019;60(3):1079–95. doi:10.1007/s00158-019-02258-y.
16. Sotoudeh-Anvari A. A critical review on theoretical drawbacks and mathematical incorrect assumptions in fuzzy OR methods: review from 2010 to 2020. Appl Soft Comput. 2020;93:106354. doi:10.1016/j.asoc.2020.106354.
17. Wang GY, Liu J, Wang YZ. Analysis of fuzzy reliability for plane sliding of slope. Rock Soil Mech. 2005;26:283–6.
18. Gupta U, Gupta D. Least squares structural twin bounded support vector machine on class scatter. Appl Intell. 2023;53(12):15321–51. doi:10.1007/s10489-022-04237-1.
19. Mirjalili S, Mirjalili SM, Lewis A. Grey wolf optimizer. Adv Eng Softw. 2014;69:46–61. doi:10.1016/j.advengsoft.2013.12.007.

20. Wong TT. Parametric methods for comparing the performance of two classification algorithms evaluated by k-fold cross validation on multiple data sets. Pattern Recogn. 2017;65:97–107. doi:10.1016/j.patcog.2016.12.018.
21. Gao G, Hazbeh O, Davoodi S, Tabasi S, Rajabi M, Ghorbani H, et al. Prediction of fracture density in a gas reservoir using robust computational approaches. Front Earth Sci. 2023;10:1023578. doi:10.3389/feart.2022.1023578.
22. Zeng Q, Zheng M, Huang D. Simulation of moving bed erosion based on theweakly compressible smoothed particle hydrodynamics-discrete element coupling method. Fluid Dyn Mater Process. 2023;19(12):2981–3005. doi:10.32604/fdmp.2023.029427.
23. Qian Q, et al. Simulation of oil-water flow in shale oil reservoirs based on smooth particle hydrodynamics. Fluid Dyn Mater Process. 2022;18(4):1089–97. doi:10.32604/fdmp.2022.019837.
24. Du X, Liu M, Sun Y. Optimization of the internal circulating fluidized bed using computational fluid dynamics technology. Fluid Dyn Mater Process. 2022;18(2):303–12. doi:10.32604/fdmp.2022.016242.
25. Huang H, Li Z, Luo J, Chang Z. On the stability of carbon shale slope under rainfall infiltration. Fluid Dyn Mater Process. 2021;17(6):1165–78. doi:10.32604/fdmp.2021.017256.
26. Altrock CV. Fuzzy logic and neurofuzzy—applications in business and finance prentice hall, New Jersey mathworks (2018a) MATLAB version 9.4.0. Natick, Massachusetts: The Mathworks, Inc.; 1995.
27. Nayak J, Swapnarekha H, Naik B, Dhiman G, Vimal S. 25 years of particle swarm optimization: flourishing voyage of two decades. Arch Comput Method E. 2023;30(3):1663–1725. doi:10.1007/s11831-022-09849-x.
28. Singh SK, Chakravarty D. Assessment of slope stability using classification and regression algorithms subjected to internal and external factors. Arch Min Sci. 2023;68(1):87–102.
29. Firincioglu BS, Ercanoglu M. Insights and perspectives into the limit equilibrium method from 2D and 3D analyses. Eng Geol. 2021;281:105968. doi:10.1016/j.enggeo.2020.105968.
30. Ribeiro RA. Fuzzy multiple attribute decision making: a review and new preference elicitation techniques. Fuzzy Set Syst. 1996;78(2):155–81. doi:10.1016/0165-0114(95)00166-2.